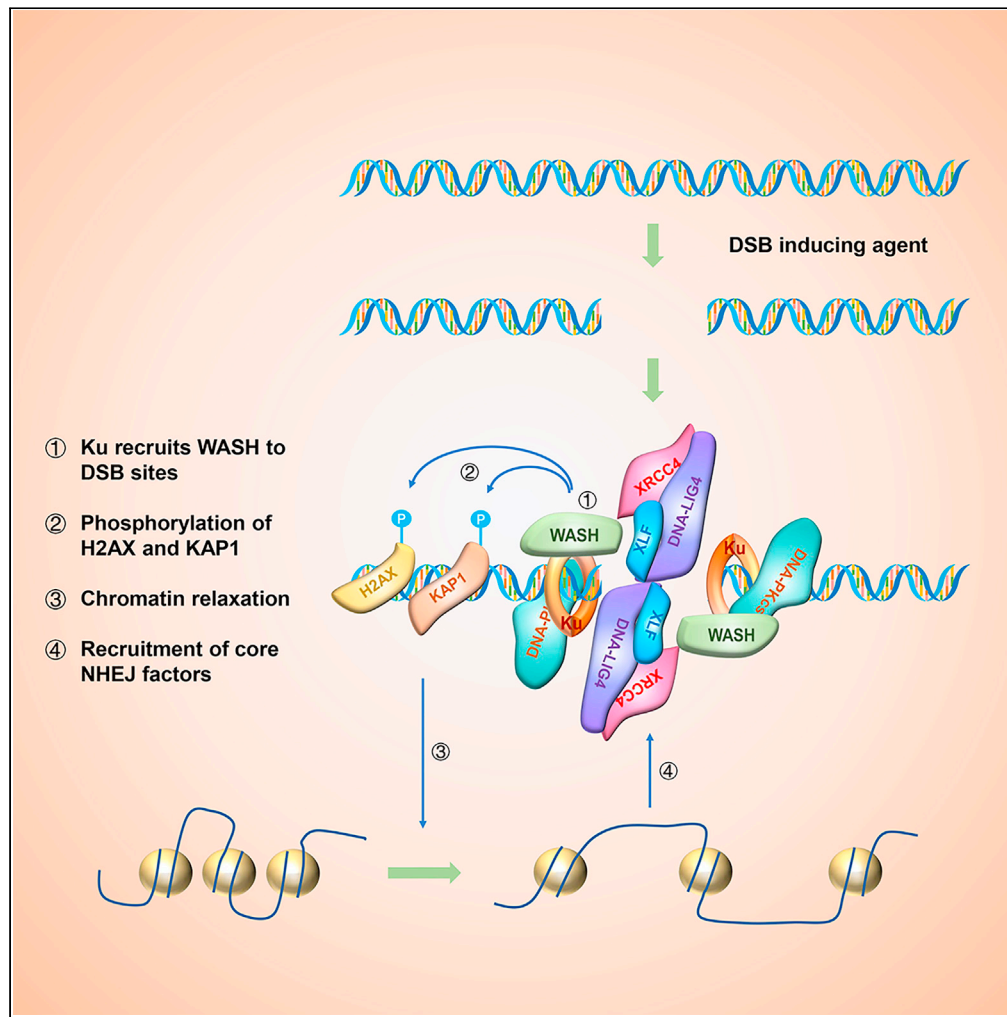**Article**

WASH interacts with Ku to regulate DNA double-stranded break repair

Tao Wang, Xiao-Hui Du, Yu Hong, ..., Jie Ge, Daniel D. Billadeau, Zhi-Hui Deng

deng.zhihui@qmu.edu.cn

Highlights

WASH localizes to DSB sites by interacting with Ku

WASH promotes DNA repair though NHEJ pathway

WASH promotes chromatin relaxation through phosphorylation of H2AX and KAP1

VCA domain is essential for WASH-dependent DSB repair

Article

WASH interacts with Ku to regulate DNA double-stranded break repair

Tao Wang,[1] Xiao-Hui Du,[1] Yu Hong,[1] Xian Hong,[1] Li Fan,[1] Jian-Wen Zhou,[1] He Sun,[1] Jie Ge,[2] Daniel D. Billadeau,[3] and Zhi-Hui Deng[1,4,*]

SUMMARY

The Wiskott-Aldrich syndrome protein and SCAR homolog (WASH), an actin nucleation-promoting factor, is present in the nucleus where it regulates gene transcription and maintains nuclear organization. Here, we show that WASH interacts with core non-homologous end-joining (NHEJ) factors including Ku70/Ku80 and DNA-PKcs, and Ku70/Ku80 is involved in the recruitment of WASH to the sites of DNA double-stranded break (DSB). WASH depletion leads to increased cell sensitivity and impaired DNA repair capacity in response to etoposide-induced DSBs and reduces NHEJ efficiency. Mechanistically, we show that loss of WASH inhibits the phosphorylation of DNA-PKcs, H2AX, and KAP1 after DSB induction and reduces chromatin relaxation and the recruitment of several downstream NHEJ factors to DSBs. Moreover, WASH role in DSB repair depends on its conserved C-terminal VCA domain and Arp2/3 activation. Our findings reveal a function and mechanistic insight for WASH in DNA DSB repair by the NHEJ pathway.

INTRODUCTION

DNA double-stranded breaks (DSBs) induced by ionizing radiation or chemotherapeutics are among the most detrimental DNA damage. DSBs lead to genome instability or cell death if not repaired in a timely fashion. Thus, effective and proper DNA repair is essential for suppression of genomic instability and subsequent malignant transformation. Eukaryotic cells have evolved two indispensable DNA repair pathways, non-homologous end-joining (NHEJ) and homologous recombination (HR) (Ceccaldi et al., 2016). In mammalian cells, the major DNA repair pathway is NHEJ, which works throughout the cell cycle. NHEJ accounts for nearly all DSB repair outside of S and G2 phases and about 80% of DSB repair within S and G2 (Beucher et al., 2009; Mao et al., 2008).

The core protein factors involved in NHEJ include Ku, DNA-dependent protein kinase catalytic subunit (DNA-PKcs), X-ray repair cross-complementing protein 4 (XRCC4), XRCC4-like factor (XLF), and DNA ligase 4. Ku is a heterodimer consisting of Ku70 and Ku80, which initially binds to the newly formed double-stranded DNA ends and is required for the recruitment of DNA-PKcs (Downs and Jackson, 2004). The recruitment of DNA-PKcs leads to the inward translocation of Ku protein and activation of DNA-PKcs kinase activity (Calsou et al., 1999; Yoo and Dynan, 1999). Although DNA-PKcs-mediated phosphorylation of core NHEJ factors including Ku70/80, XRCC4, XLF, and DNA ligase 4 is not essential for NHEJ (Douglas et al., 2005; Wang et al., 2004; Yu et al., 2003, 2008), it has been demonstrated that DNA-PKcs kinase activity is required for the efficient progression of NHEJ reactions (Kienker et al., 2000; Kurimasa et al., 1999). The two broken DNA ends are ultimately ligated by XRCC4 and DNA ligase 4 (Critchlow et al., 1997), and the activity of which is promoted by the co-factor XLF (Ahnesorg et al., 2006; Lu et al., 2007; Tsai et al., 2007).

Wiskott-Aldrich syndrome protein and SCAR homolog (WASH) is a member of the Wiskott-Aldrich syndrome protein (WASP) family and exists in a pentameric complex comprising WASH, FAM21, SWIP, Strumpellin, and CCDC53 (Derivery et al., 2009; Gomez and Billadeau, 2009; Jia et al., 2010). WASH has been reported to regulate retromer-dependent endosomal sorting and trafficking through facilitating the generation of branched filamentous actin (F-actin) on endosomes (Duleh and Welch, 2010, 2012; Gomez and Billadeau, 2009; Hao et al., 2013). Similar to other WASP family members, WASH promotes actin filament nucleation by the actin-related protein 2/3 (Arp2/3) complex through its conserved C-terminal VCA (verprolin, central, acid) domain (Linardopoulou et al., 2007; Liu et al., 2009). Recently, roles for WASH and

[1]Laboratory of Protein Structure and Function, Institute of Medicine and Pharmacy, Qiqihar Medical University, Qiqihar, Heilongjiang 161006, China

[2]Department of Epidemiology and Statistics, School of Public Health, Qiqihar Medical University, Qiqihar, Heilongjiang 161006, China

[3]Division of Oncology Research and Schulze Center for Novel Therapeutics, Mayo Clinic College of Medicine, Rochester, MN 55905, USA

[4]Lead contact

*Correspondence:
deng.zhihui@qmu.edu.cn

https://doi.org/10.1016/j.isci.2021.103676

its complex components in the nucleus are beginning to emerge (Deng et al., 2015; Verboon et al., 2015; Xia et al., 2014, 2017). Notably, a recent study in *Drosophila* cells has demonstrated that nuclear F-actin assembled at DSB sites by the Arp2/3 complex is required for relocalization of heterochromatic breaks to the nuclear periphery and subsequent heterochromatin repair, and depletion of WASH causes a relocalization defect, suggesting WASH might be involved in DNA DSB repair (Caridi et al., 2018).

To further define putative nuclear functions of WASH, we isolated nuclear WASH and performed mass spectrometry to identifying WASH-interacting proteins. Here we report that WASH interacts with components of the NHEJ machinery including DNA-PKcs, Ku70, Ku80, XRCC4, and DNA ligase 4. Significantly, we show that Ku70/Ku80 is required for the recruitment of WASH to sites of DSB and that WASH promotes DNA DSB repair through NHEJ. Our results reveal a role and mechanism for WASH in regulating DSB repair and suggest a potential function for nuclear WASH in the maintenance of genomic stability.

RESULTS

WASH interacts with Ku protein

To better characterize the function of nuclear WASH, we first constructed a plasmid expressing nuclear WASH, named HA-YFP-NLS.WASH, by inserting the SV40 nuclear localization sequence (NLS) between HA-YFP tag and the WASH coding sequence (CDS). As expected, HA-YFP-NLS.WASH was mainly localized to the nucleus (Figure 1A). To gain insight into nuclear WASH function, we expressed this expression plasmid in HEK-293T cells, purified HA-YFP-NLS.WASH from nuclear extracts using anti-HA antibody, and identified potential interacting partners by mass spectrometry (MS) (Table S1). Next, we performed KEGG pathway and Gene Ontology (GO) analysis to functionally analyze the top 100 scored candidate proteins identified by MS, using DAVID Bioinformatics Resources 6.8 (https://david.ncifcrf.gov/). Notably, both KEGG pathway and GO analysis showed an NHEJ DNA repair pathway (Figure S1). The proteins involved in the NHEJ pathway included DNA-PKcs, Ku70, Ku80, XRCC4, and DNA ligase 4 (Figure 1B).

Owing to the essential roles for Ku protein in the initial DNA DSB recognition and recruitment of other NHEJ factors to the DSB (Fell and Schild-Poulter, 2015), we mainly concentrated on the putative interaction of WASH with Ku. As shown in Figure 1C, endogenous WASH readily co-immunoprecipitated endogenous Ku70, Ku80, and DNA-PKcs from HEK-293T cells. Moreover, these interactions were unlikely bridged by DNA, since ethidium bromide (EtBr) treatment, which disrupts the majority of protein-DNA interactions, did not affect the co-immunoprecipitation (Figure 1C). Consistent with this, both overexpressed HA-YFP.WASH and HA-YFP-NLS.WASH co-immunoprecipitated endogenous Ku70 and Ku 80 (Figure 1D), and co-immunoprecipitation showed WASH primarily interacts with Ku in the nuclear fraction (Figure S2). To further define the subcellular localization of the interaction between WASH and Ku, we performed an *in situ* proximity ligation assay (PLA). Co-staining WASH with Ku70 or Ku80 showed robust PLA signal (red signal) generation in the nucleus in contrast to IgG-treated control cells, and no significant change in the number of PLA foci was observed after etoposide treatment (Figures 1E and 1F). Taken together, the interaction of WASH with Ku protein is constitutive and specific in the nucleus.

Ku recruits WASH to DNA damage sites

It has been established that the Ku70/Ku80 heterodimer directly recognizes broken DNA ends as a DSB sensor and recruits numerous NHEJ factors to DSBs (Fell and Schild-Poulter, 2015; Yang et al., 2018). Given the interaction between WASH and Ku heterodimer, it prompted us to examine if WASH is recruited to DNA breaks. To this end, we transiently expressed YFP-NLS.WASH in HEK-293T cells and examined the recruitment kinetics of nuclear WASH to the DSBs induced by laser micro-irradiation. Notably, the recruitment of YFP-NLS.WASH to the laser-induced damage tracks was clearly observed after micro-irradiation within 10 s (Figure 2A). Furthermore, YFP-NLS.WASH rapidly reached the irradiated nuclear region simultaneously with mCherry-Ku70 (Figure S3). Next, to further test whether Ku protein is required for recruitment of WASH, we depleted Ku in HEK-293T using two small interfering RNAs (siRNAs) that, respectively, target the CDS and untranslated region (UTR) of Ku70 (Figure 2B). As expected, depletion of Ku70 also resulted in the loss of Ku80 (Figure 2B). We then asked whether depletion of Ku70 affected the recruitment of WASH to DSBs. As shown in Figures 2C and 2D, Ku70 depletion resulted in markedly reduced recruitment of nuclear WASH to laser-induced damage tracks. Importantly, re-expression of mCherry-Ku70 in si-Ku70.UTR-silenced cells restored the recruitment of WASH to DSB sites (Figures 2C and 2D). However, depletion of WASH did not affect the recruitment of Ku70 and DNA-PKcs to DSBs (Figures 2E–2G, and
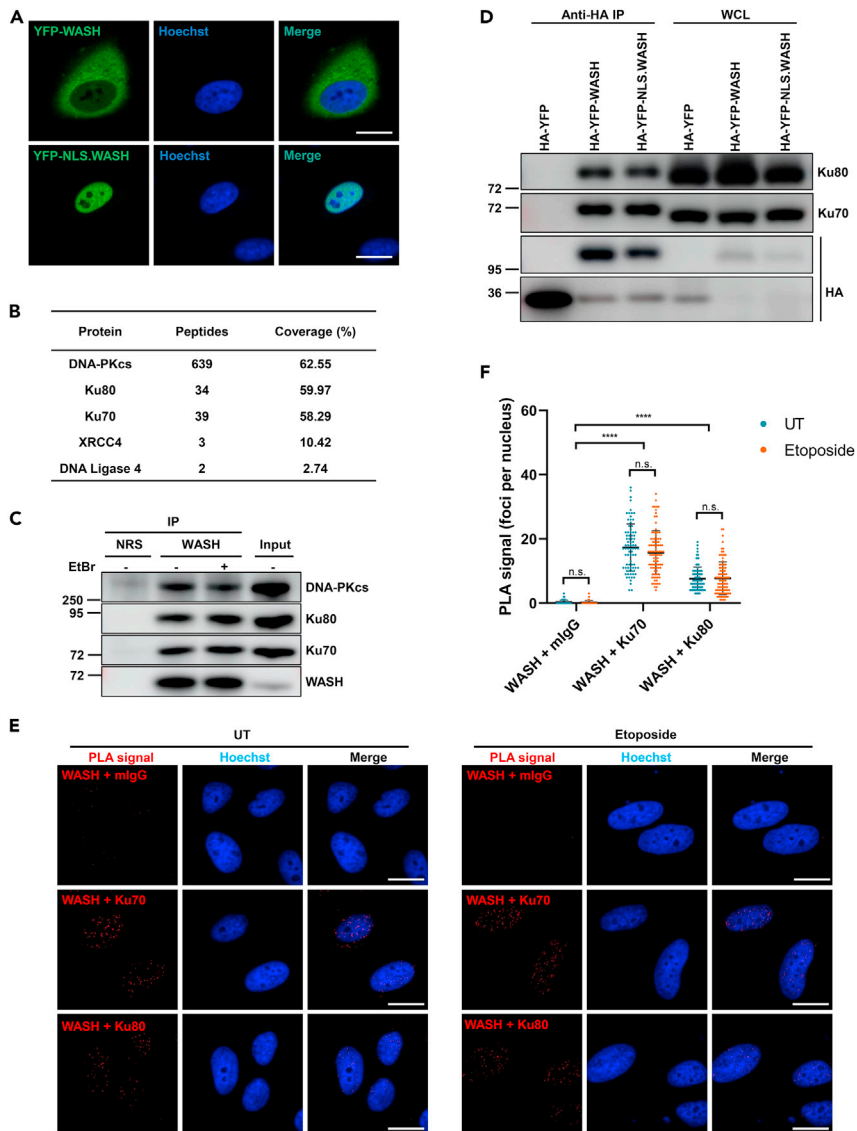
Figure 1. WASH interacts with Ku protein

(A) HeLa cells were transfected with HA-YFP.WASH and HA-YFP-NLS.WASH for YFP fluorescence imaging. Scale bar: 20 μm.

(B) The nuclear proteins were extracted from HEK-293T cells expressing HA-YFP-NLS.WASH, subjected to subsequent anti-HA affinity purification, and analyzed by mass spectrometry. NHEJ factors associated with WASH identified by mass spectrometry are shown.

(C) The interactions between endogenous WASH and Ku70/Ku80/DNA-PKcs were determined by co-immunoprecipitation (Co-IP) assay. HEK-293T cell lysates were immunoprecipitated in the absence or presence of EtBr (0.2 mg/mL) with normal rabbit serum (NRS) or anti-WASH followed by SDS-PAGE and immunoblotting.

(D) The interactions between WASH and Ku70/Ku80 were confirmed by Co-IP assay. HEK-293T cells expressing the HA-YFP, HA-YFP.WASH, or HA-YFP-NLS.WASH were lysed and subjected to subsequent anti-HA co-immunoprecipitation followed by SDS-PAGE and immunoblotting.

(E) The interactions between WASH and Ku70/Ku80 were assessed by PLA with the indicated pairs of primary antibodies in HeLa cells with 50 μM etoposide treatment for 2 h or not. Co-staining WASH with mouse IgG was used as negative control. Scale bar: 20 μm.

(F) PLA signal foci numbers per nucleus for 81–123 cells of each group were calculated and presented as mean $\pm$ SD. Unpaired t test was performed between etoposide-treated and untreated groups. Two-way analysis of variance (ANOVA) with Dunnett's multiple comparisons test was performed among mIgG, Ku70, and Ku80 groups. ****, $p < 0.0001$; n.s., not significant. See also Figures S1 and S2.
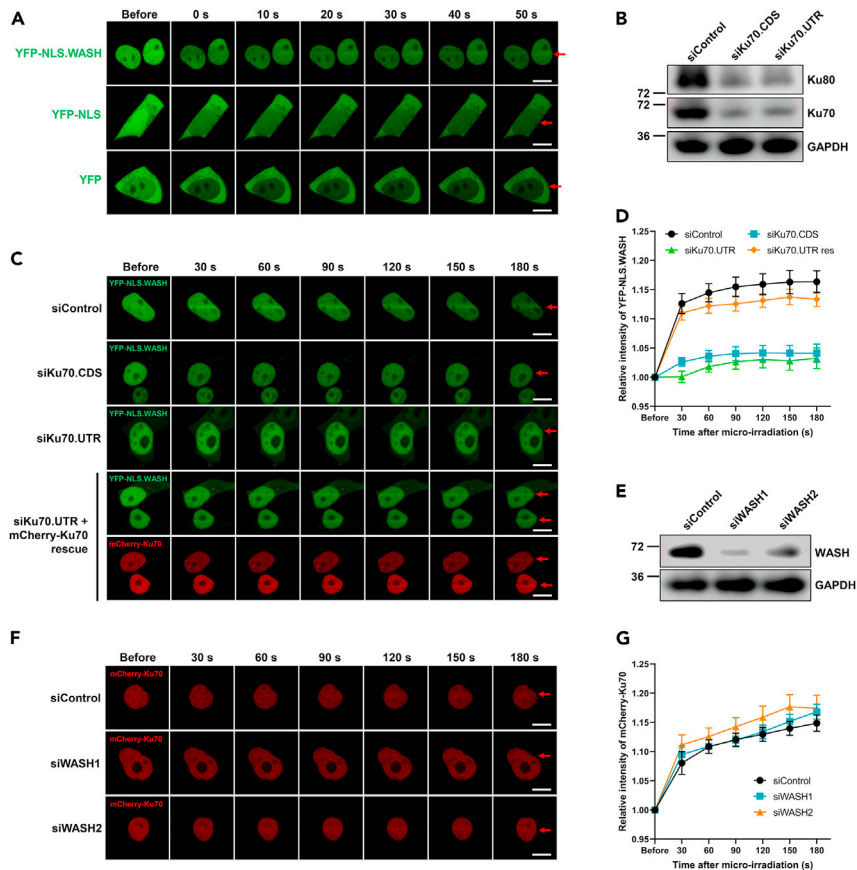
Figure 2. WASH recruitment to DNA damage sites is dependent on Ku protein

(A) Laser micro-irradiation was used to induce DNA damage in a line pattern in HEK-293T cells transfected with YFP, YFP-NLS, or YFP-NLS.WASH respectively. Scale bar: 10 μm.

(B) Expression levels of Ku70 and Ku80 in HEK-293T cells transfected with either control siRNA (siControl) or siRNAs targeting Ku70 were examined by immunoblot.

(C) Recruitment of nuclear WASH to laser-generated DNA damage sites is attenuated by siRNA-mediated knockdown of Ku70 in HEK-293T cells, and re-expression of Ku70 in siKu70.UTR-silenced cells restored the recruitment of WASH. Scale bar: 10 μm.

(D) Quantification of nuclear WASH recruitment to DNA damage tracks in control and Ku70-depleted cells. The relocation kinetics of nuclear WASH to DNA damage sites was monitored in a time course as indicated. The results are presented as mean ± SEM.
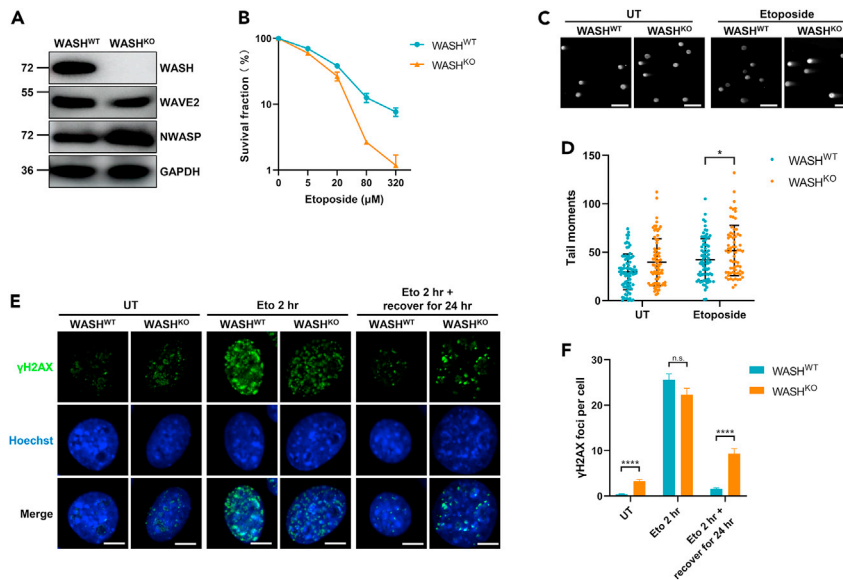
(E) Expression of WASH was examined by immunoblot.

(F) Recruitment of mCherry-Ku70 to laser-generated DNA damage sites is not affected by siRNA-mediated depletion of WASH. Scale bar: 10 μm.

(G) Quantification of mCherry-Ku70 recruitment to laser-induced DNA damage sites in control and WASH-suppressed cells. The results are presented as mean ± SEM. See also Figures S3 and S4.

S4), suggesting WASH is dispensable for Ku and DNA-PKcs recruitment. Taken together, these results indicate that the recruitment of WASH to DSBs is dependent on Ku70/Ku80.

WASH promotes cell survival and DNA repair after DSB induction

Since WASH localizes to DSB sites, we asked whether it is required for DNA repair. To this end, we constructed a WASH knockout (WASH^{KO}) 3T3 cell line using the CRISPR-Cas9 system and showed that WASH knockout did not affect the expression of other WASP family proteins such as NWASP and WAVE (Figure 3A), as well as normal cell cycle (Figure S5). Next, we treated wild-type (WASH^{WT}) cells or WASH^{KO} cells with etoposide, a topoisomerase II inhibitor that induces DSBs and assessed viability using the colony formation assay. Significantly, WASH^{KO} cells were more sensitive to etoposide than WASH^{WT} cells,

Figure 3. WASH Knockout impairs DNA repair capacity

(A) Expression levels of WASH, WAVE2, and NWASP in WASH^{WT} and WASH^{KO} 3T3 cells were measured by immunoblot.

(B) WASH^{WT} cells and WASH^{KO} cells treated with indicated concentration of etoposide for 6 h were plated for colony formation assay. Survival fractions were normalized to the colony number of cells without etoposide treatment. Data were presented as mean ± SD.

(C) WASH^{WT} and WASH^{KO} 3T3 cells treated with 50 μM etoposide for 60 min were allowed to recover for 30 min. Neutral Comet assay was performed to assess the DSB repair capacity. Scale bar: 100 μm.

(D) Tail moments for 67–84 cells of each group were calculated. Data are presented as mean ± SD. Unpaired t test was performed between WASH^{WT} and WASH^{KO}. *, p < 0.05.

(E) Representative γH2AX foci of WASH^{WT} and WASH^{KO} 3T3 cells after etoposide treatment. 3T3 cells treated with 50 μM etoposide for 2 h were allowed to recover for 0 or 24 h under normal growth conditions, and then γH2AX foci were assessed. Scale bar: 10 μm.

(F) γH2AX foci numbers per cell for 63–152 cells of each group were calculated and presented as mean ± SEM. Unpaired t test was performed between WASH^{WT} and WASH^{KO}. ****, p < 0.0001; n.s., not significant. See also Figures S5 and S6.

suggesting WASH is required for cell survival in response to DSBs (Figure 3B). To confirm a role for WASH in repairing DSBs, we performed the neutral Comet assay. WASH^{KO} cells showed more unrepaired DSBs compared with WASH^{WT} cells, indicating that WASH deletion reduces the rates of DSB repair (Figures 3C and 3D). Next, we assessed the resolution of etoposide-induced γH2AX (phosphorylation of the histone variant H2AX at serine 139) foci, which serve as a biomarker of DSBs, and γH2AX will persist if DSBs are not repaired. WASH^{KO} cells displayed increased foci number and fluorescence intensity of γH2AX without genomic insult when compared with WASH^{WT} cells, suggesting that WASH knockout results in spontaneous DNA damage and genomic instability (Figures 3E, 3F, and S6A). Interestingly, knocking out of WASH did not change etoposide-induced γH2AX foci formation/numbers after etoposide treatment for 2 h (Figures 3E and 3F), although a decrease in γH2AX fluorescence intensity was observed in WASH^{KO} cells (Figure S6A). However, after 24 h of recovery post etoposide treatment, γH2AX foci resolution was dramatically attenuated in the WASH^{KO} cells, suggesting that WASH is involved in the DSB repair (Figures 3E, 3F, and S6A). Consistent with this, stable knockdown of WASH (shWASH) in HeLa cells showed a similar elevation of γH2AX foci numbers compared with the shRNA control (shControl) cells after 24 h of recovery post etoposide treatment (Figures S6B–S6D). Collectively, these observations led to a conclusion that WASH is required for efficient repair of DNA DSBs.

WASH is required for chromatin relaxation

Recently, it was shown that the phosphorylation of H2AX and KAP1 by DNA-PKcs is required for chromatin relaxation, which allows access of condensed genomic DNA to DNA repair machinery following DSB formation (Lu et al., 2019; Nakamura et al., 2010; Ziv et al., 2006). Of note, we observed a marked decrease in the signal intensity of γH2AX in WASH^{KO} cells after treatment with etoposide for 2 h (Figures 3E and
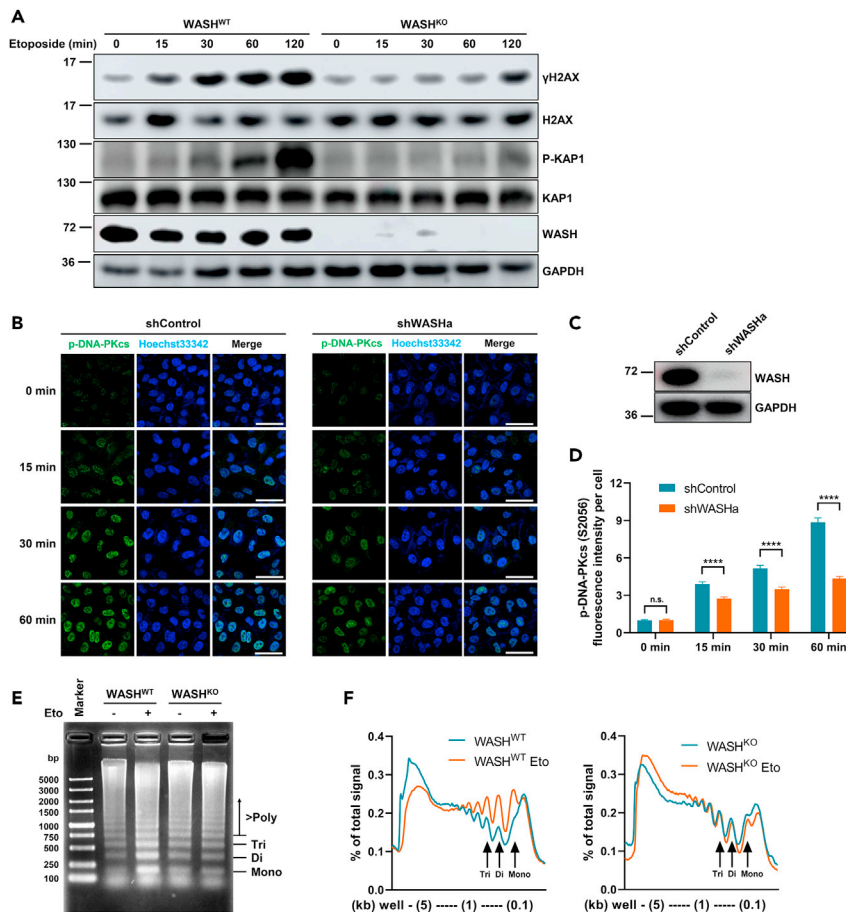
Figure 4. WASH is required for DNA relaxation

(A) WASH^{WT} and WASH^{KO} 3T3 cells were treated with 50 μM etoposide for the indicated time. Whole-cell lysates were obtained and immunoblotted with the indicated antibodies. GAPDH serves as a loading control.

(B) Representative phosphorylation of DNA-PKcs (S2056) of shControl and shWASHa HeLa cells after etoposide treatment. HeLa cells stably expressing lentiviral shRNA against WASH or control shRNA were treated with 50 μM etoposide for 0, 15, 30, or 60 min. Then fluorescence intensity of p-DNA-PKcs (S2056) was assessed. Scale bar: 50 μm.
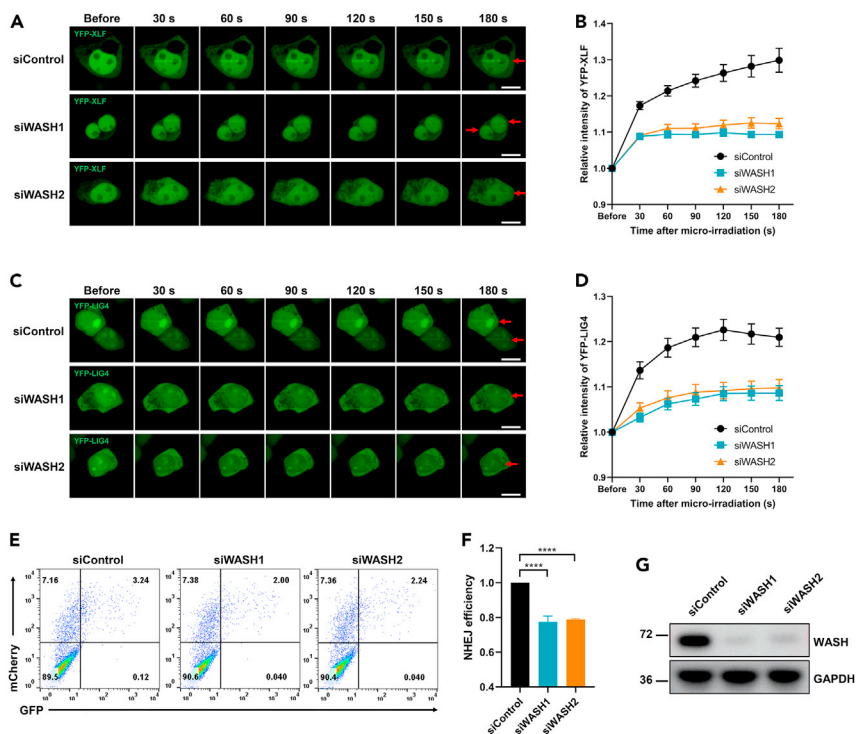
(C) Expression levels of WASH in shControl and shWASHa HeLa cells were examined by immunoblot.

(D) Fluorescence intensity of p-DNA-PKcs (S2056) per cell for 169–247 cells of each group were calculated and presented as mean ± SEM. Unpaired t test was performed between shControl and shWASHa. ****, p < 0.0001; n.s., not significant.

(E) Chromatin relaxation induced by etoposide is lessened in the WASH^{KO} cells. 3T3 WASH^{WT} and WASH^{KO} cells were treated with 50 μM etoposide for 60 min. Accessibility of chromatin was then measured by MNase digestion assay.

(F) Quantified signal of the various gel lanes presented in (E).

S6A), and this observation led us to hypothesize that WASH participates in the phosphorylation of H2AX and KAP1 and subsequent DNA relaxation. To test this hypothesis, we examined the influence of WASH on the phosphorylation of H2AX and KAP1 (pS824) after etoposide treatment. The phosphorylation of H2AX and KAP1 in WASH^{KO} cells was dramatically decreased compared with WASH^{WT} cells after etoposide treatment (Figure 4A). In addition, we found that WASH knockdown reduced etoposide-induced phosphorylation of DNA-PKcs at Ser2056, one of the prominent autophosphorylation sites of DNA-PKcs after DSB induction (Chen et al., 2005), suggesting that WASH regulates the phosphorylation of H2AX and KAP1 through DNA-PKcs activation (Figures 4B–4D). Next, we examined the function of WASH in chromatin relaxation after DSB induction using the Micrococcal Nuclease (MNase) digestion assay. MNase preferentially cuts the DNA in the linker regions between nucleosomes, and thus the efficiency of MNase digestion depends on the degree of chromatin relaxation. Consistent with previous observations that DSBs induce an increase in chromatin relaxation (Lu et al., 2019; Nakamura et al., 2010; Ziv et al., 2006), etoposide treatment caused a marked increase in cellular chromatin accessibility to MNase in WASH^{WT} cells (Figures

Figure 5. WASH promotes DNA DSB repair by NHEJ pathway

(A) Recruitment of YFP-XLF to laser-generated DNA DSBs is attenuated by siRNA-mediated depletion of WASH. Scale bar: 10 μm.

(B) Quantification of YFP-XLF recruitment to laser-induced DNA damage tracks in siControl and siWASH cells. The relocation kinetics of YFP-XLF to damaged DNA sites was monitored in a time course as indicated. The results are presented as mean ± SEM.

(C) Recruitment of YFP-DNA ligase 4 (LIG4) to laser-generated DNA DSBs is attenuated by siRNA-mediated depletion of WASH. Scale bar: 10 μm.

(D) Quantification of YFP-LIG4 recruitment to laser-induced DNA damage tracks in siControl and siWASH cells. The results are presented as mean ± SEM.

(E) HEK-293T cells transfected with the indicated siRNA were subjected to NHEJ assay.

(F) NHEJ efficiency was calculated by comparing the number of GFP-positive cells with the number of mCherry-positive cells. Data were presented as mean ± SD. One-way ANOVA with Dunnett's multiple comparisons test was performed among siControl, siWASH1, and siWASH2. ****, $p < 0.0001$.

(G) Expression levels of WASH in HEK-293T cells transfected with either siControl or siRNAs targeting WASH were examined by immunoblot. See also Figure S7.

4E and 4F). However, this increased MNase accessibility was attenuated in the WASH[KO] cells (Figures 4E and 4F). Collectively, these results indicate that WASH is responsible for chromatin relaxation after DSB formation.

WASH promotes DSB repair by NHEJ pathway

Chromatin relaxation makes the area surrounding DSBs more approachable for DNA repair proteins including core NHEJ factors such as XRCC4 and XLF (Lu et al., 2019). We therefore tested the recruitment of core NHEJ proteins to DSBs induced by laser micro-irradiation in siControl- and siWASH-treated cells. Consistent with the function of WASH in chromatin relaxation, depletion of WASH led to decreased recruitment of XLF and DNA ligase 4 to DNA damage generated by laser micro-irradiation, suggesting that WASH is required for the localization of downstream NHEJ factors to damaged DNA (Figures 5A–5D). However, given that chromatin remodeling makes condensed DNA more accessible for repair proteins including HR factors (Lu et al., 2019), our data cannot exclude the possibility that WASH may facilitate DNA repair by the assembling HR machinery at DSBs. To further verify the effect of WASH on NHEJ and HR repair pathways, two well-characterized GFP-based reporter systems, EJ5-GFP and DR-GFP, were

utilized to evaluate DSB repair efficiency. We found that WASH knockdown reduced the efficiency of the NHEJ, but not HR repair pathway, suggesting that WASH primarily participates in the NHEJ repair pathway (Figures 5E–5G and S7). Taken together, these data indicate that WASH promotes DSB repair primarily by the NHEJ pathway.

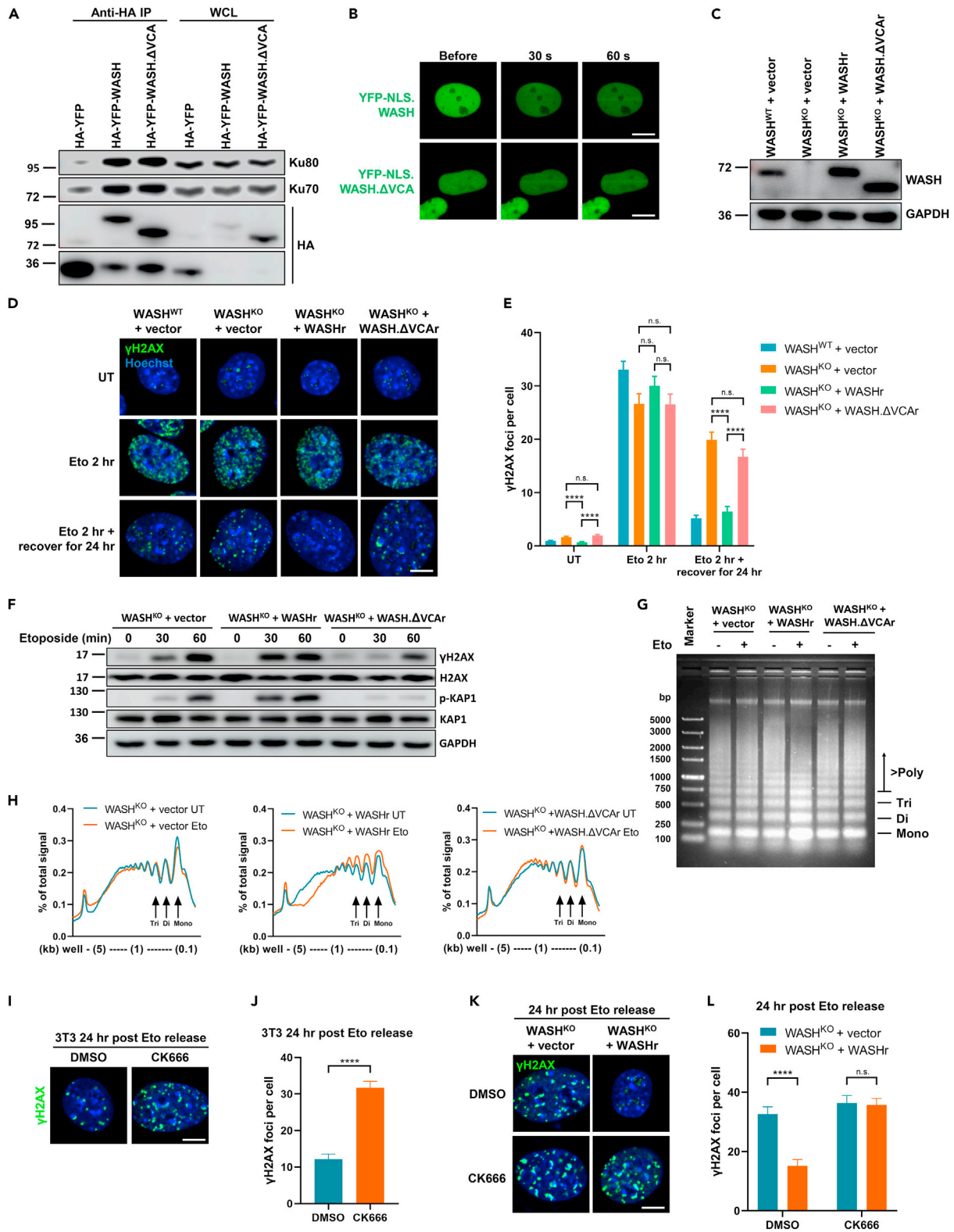### VCA domain is essential for WASH-dependent DSB repair

The VCA domain of WASH is necessary and sufficient to stimulate actin polymerization by the Arp2/3 complex (Linardopoulou et al., 2007; Liu et al., 2009). Notably, recent studies showed a direct link of nuclear Arp2/3 and F-actin with DSB repair (Caridi et al., 2018; Schrank et al., 2018). These observations prompted us to examine whether the role of WASH in DSB repair is VCA and Arp2/3 dependent. We found the truncated WASH protein lacking the VCA domain (WASH.ΔVCA) still interacts with Ku protein (Figure 6A) and nuclear WASH.ΔVCA is recruited to DNA lesions generated by micro-irradiation (Figure 6B), suggesting that the VCA domain is dispensable for the WASH:Ku interaction and recruitment of WASH to DSB sites. To further test the role of the VCA domain in WASH-dependent DSB repair, we stably overexpressed vector in WASH^{WT} 3T3 cells, and vector, wild type, or VCA-depleted (ΔVCA) mouse WASH in WASH^{KO} 3T3 cells using a lentivirus-mediated stable overexpression system (Figure 6C). Intriguingly, restoring wild-type WASH rescued the deficiency of WASH^{KO} cells in γH2AX foci resolution after etoposide treatment, but WASH.ΔVCA-rescued cells failed to restore this deficiency (Figures 6D and 6E). Similarly, WASH.ΔVCA-rescued cells did not restore the phosphorylated levels of H2AX and KAP1 as well as chromatin relaxation in WASH^{KO} cells after etoposide-induced DSB (Figures 6F–6H), indicating that the role of WASH in chromatin relaxation depends on its VCA domain. Moreover, treatment with CK666, an Arp2/3 complex inhibitor, resulted in greater numbers of persistent γH2AX foci (Figures 6I and 6J) and prevented the ability of γH2AX foci resolution in WASH-rescued WASH^{KO} cells (Figures 6K and 6L). These observations suggest that WASH plays essential roles in DSB repair through its VCA domain-dependent Arp2/3 activation.

DISCUSSION

In this study, we have identified the interaction between WASH and Ku protein. We further show that WASH is rapidly recruited by Ku protein to DSB sites and promotes DNA DSB repair by NHEJ. Moreover, our findings indicate that WASH is involved in the activation of DNA-PKcs and the phosphorylation of H2AX and KAP1 and promotes chromatin relaxation after DSB induction. Notably, the VCA domain is crucial for the role of WASH in DNA damage repair. These observations provide mechanistic insights into the role of WASH in DNA damage repair. Given that DSBs are deleterious DNA lesions, our findings suggest that WASH likely participates in the regulation of cell survival, the maintenance of genomic integrity, and possibly the prevention of tumorigenesis in response to DSBs.

Nuclear WASH has been reported to localize at the promoter of the mouse *c-Myc* gene in hematopoietic stem cells (Xia et al., 2014). Moreover, our previous study indicated that nuclear FAM21, a key component of WASH complex, interacts with the promoter regions of multiple NF-κB target genes in HeLa cells (Deng et al., 2015). However, we find here that WASH interacts with Ku protein independently of protein-DNA interactions, as EtBr treatment did not impair their interaction. Although WASH and Ku were rapidly recruited to DNA lesions generated by micro-irradiation, our data indicate that depletion of WASH does not affect Ku recruitment to DSBs but instead Ku70/Ku80 are involved in the recruitment of WASH to sites of DSB. Intriguingly, WASH is able to promote the recruitment of downstream NHEJ factors including XLF and DNA ligase 4, but not DNA-PKcs, to damaged DNA sites. Of note, the Ku70/Ku80 heterodimer rapidly recognizes the ends of DSBs in a sequence-independent manner and acts as a scaffold for the recruitment of other core factors as well as accessory NHEJ proteins such as APLF, WRN, Polymerase μ, and λ (Fell and Schild-Poulter, 2015). Whether WASH is involved in the recruitment of these accessory NHEJ factors to DSBs remains to be determined.

Similar to the recruitment of WASH to DSB sites, WASP, another key WASP family protein, was reported to accumulate at DSBs in U2OS cells (Schrank et al., 2018). WASP facilitates homology-directed repair by mediating F-actin formation via activation of the Arp2/3 complex (Schrank et al., 2018). In addition, as WASP regulates RNA polymerase II-dependent transcription, WASP-deficient cells displayed R-loop accumulation and R-loop-mediated DSBs suggesting that WASP promotes DSB repair via regulation of gene transcription (Sarkar et al., 2018). However, we show that WASH promotes DSB repair by the NHEJ pathway that is mechanistically distinct from WASP. Therefore, these data consolidate the idea that WASP family proteins play essential roles in DSB repair through distinct DNA-repair pathways. Furthermore, similar to

Figure 6. VCA domain is required for WASH-dependent DSB repair

(A) VCA domain is dispensable for the interaction between WASH and Ku protein. HEK-293T cells expressing the HA-YFP, HA-YFP.WASH, or HA-YFP-VCA-depleted WASH (WASH.ΔVCA) were lysed and subjected to subsequent anti-HA co-immunoprecipitation followed by SDS-PAGE and immunoblotting with indicated antibodies.

(B) VCA domain is dispensable for the recruitment of WASH to DNA damage generated by laser micro-irradiation. Laser micro-irradiation was used to induce DNA damage in HEK-293T cells expressing YFP-NLS.WASH or YFP-NLS.WASH.ΔVCA, respectively. Scale bar: 10 μm.

(C) Generation of 3T3 cells stably expressing vector and 3T3 WASH^{KO} cells stably expressing vector, WASH, or WASH.ΔVCA. Expression levels of WASH protein in 3T3 stable cell lines were detected by immunoblot.

(D) Representative γH2AX foci of 3T3 stable cells after etoposide treatment. 3T3 stable cells treated with 50 μM etoposide for 2 h were allowed to recover for 0 or 24 h under normal growth conditions, and then γH2AX foci were assessed. Scale bar: 10 μm.

(E) γH2AX foci numbers per cell for 102–216 cells of each group were calculated and presented as mean ± SEM. One-way ANOVA with Dunnett's multiple comparisons test was performed among WASH^{WT} + vector, WASH^{KO} + vector, WASH^{KO} + WASHr, and WASH ^{KO} + WASH.ΔVCAr. ****, p < 0.0001; n.s., not significant.

(F) 3T3 stable cells were treated with 50 μM etoposide for the indicated time. Whole-cell lysates were obtained and immunoblotted with the indicated antibodies. GAPDH serves as a loading control.

(G) Chromatin relaxation induced by etoposide is measured by MNase digestion assay. 3T3 stable cells were treated with 50 μM etoposide for 60 min followed by MNase digestion assay.

(H) Quantified signal of the various gel lanes presented in (G).

(I) Representative γH2AX foci of 3T3 cells post etoposide treatment in the presence of DMSO or CK666. 3T3 cells were pretreated with 100 μM CK666 for 1 h, treated with 50 μM etoposide for 2 h in the presence of 100 μM CK666, and allowed to recover for 24 h in fresh media containing 100 μM CK666. Control cells were treated with an equal volume of DMSO for replacing CK666. Scale bar: 10 μm.

(J) γH2AX foci numbers per cell for 89–92 cells of each group presented in (I) were calculated and presented as mean ± SEM. Unpaired t test was performed between DMSO and CK666. ****, p < 0.0001; n.s., not significant.

(K) Representative γH2AX foci of 3T3 WASH^{KO} stable cells post etoposide treatment in the presence of DMSO or CK666. 3T3 WASH^{KO} + vector and WASH^{KO} + WASHr cells were treated as in (I). Scale bar: 10 μm.

(L) γH2AX foci numbers per cell for 38–57 cells of each group presented in (K) were calculated and presented as mean ± SEM. Unpaired t test was performed between WASH^{KO} + vector and WASH^{KO} + WASHr. ****, p < 0.0001; n.s., not significant.

WASP, we also find that WASH^{KO} cells show an increase in spontaneous DSBs under unperturbed conditions, suggesting WASP family proteins play an important physiologic role in the maintenance of genomic integrity. Of note, we observed that depletion of the VCA domain attenuated WASH-dependent DSB repair and chromatin relaxation, and inhibition of Arp2/3 reduced the repair efficiency of WASH-rescued WASH^{KO} cells. These findings suggest that the role of WASH in DSB repair depends on Arp2/3-mediated actin polymerization, which is consistent with the recent reports that nuclear Arp2/3 and F-actin are essential for DSB repair (Caridi et al., 2018; Schrank et al., 2018).

Chromatin remodeling promotes the formation of relaxed chromatin structures at DSBs allowing access to the DNA-repair machinery (Price and D'Andrea, 2013). Phosphorylation of the histone variant H2AX and KAP1 are key modifications that generate an accessible state of chromatin resulting in the recruitment of DNA repair factors (Lu et al., 2019; Nakamura et al., 2010; Ziv et al., 2006). It has been reported that both DNA-PKcs and ataxia telangiectasia mutated (ATM), two members of the phosphatidylinositol 3-kinase-related kinase (PI3KK) family, are responsible for phosphorylating H2AX and KAP1 following DSB induction. Since DNA-PKcs is recruited to these sites faster than ATM (Davis et al., 2010), a recent study has verified that DNA-PKcs, but not ATM, mediates DSB-induced chromatin relaxation at early time points by phosphorylating H2AX and KAP1 (Lu et al., 2019). Although WASH does not affect DNA-PKcs recruitment to laser-generated DSBs, WASH knockdown markedly inhibits the etoposide-induced DNA-PKcs activation. Consistently, knocking out WASH dramatically reduces the phosphorylated levels of H2AX and KAP1 as well as chromatin relaxation after etoposide treatment. Thus, our findings support a notion that WASH might function as a chromatin remodeling factor to promote chromatin relaxation through H2AX and KAP1 phosphorylation by DNA-PKcs after DSB induction, which is in support of the rapid recruitment of WASH to DSB sites. How WASH contributes to chromatin remodeling is not clear. Nonetheless, it has been reported that nuclear actin and several actin-related proteins (ARPs) exist in multiple chromatin-modifying complexes, including INO80, SWR1, nucleosomal acetyltransferase of H4 (NuA4), and BRG- or Brm-associated factors (BAF) (Galarneau et al., 2000; Kapoor and Shen, 2014; Mizuguchi et al., 2004; Shen et al., 2000; Zhao et al., 1998), which are also involved in DNA damage repair (Attikum and Gasser, 2005; Chambers and Downs, 2012; Fritsch et al., 2004; Gerhold and Gasser, 2014; Kapoor et al., 2013; Morrison et al., 2004). Moreover, our findings indicate that the VCA domain of WASH is essential for chromatin relaxation and that Arp2/3 activation is involved in WASH-mediated DSB repair, suggesting WASH and these chromatin-modifying complexes could work together to regulate chromatin relaxation in response to DSBs.

In addition, we observed that WASH depletion causes a defect in recruitment of XLF to laser-induced DNA lesion. XLF, an essential core NHEJ factor, stimulates the ligation activity of the XRCC4-DNA ligase 4 complex *in vitro*, especially at mismatched DNA ends, and promotes NHEJ *in vivo* (Ahnesorg et al., 2006; Lu et al., 2007; Tsai et al., 2007). Notably, structural studies have shown that an XLF dimer interacts with an XRCC4 dimer to form extended filaments of alternating XRCC4/XLF dimers (Andres et al., 2012; Hammel et al., 2011; Reid et al., 2015; Ropars et al., 2011) and these filaments bridge and stabilize DNA ends (Andres et al., 2012). XRCC4/XLF filaments are reminiscent of nuclear Arp2/3- and NPF-dependent filamentous actin, which also localizes to DSB sites and participates in DSB repair (Caridi et al., 2018; Schrank et al., 2018). Whether nuclear actin filaments are involved in stabilizing or bridging DSBs through an interaction with XRCC4/XLF filaments will require further investigation.

In summary, this study demonstrates that WASH plays an essential role in chromatin remodeling and DSB repair via NHEJ, expanding our understanding of WASH roles in cell survival and maintaining genomic integrity in response to DSBs. Future investigations focused on how WASH contributes to DNA-PKcs activation will provide new insights into the mechanisms by which WASH regulates NHEJ.

Limitations of the study

In this study we showed that the VCA domain of WASH is essential for WASH-dependent DSB repair, but not for the WASH:Ku interaction, and that WASH is involved in DNA-PKcs activation. Further investigations are necessary to map the interaction domains between WASH and Ku70/Ku80 or DNA-PKcs, which will help to address the mechanisms by which WASH regulates NHEJ.

STAR★METHODS

Detailed methods are provided in the online version of this paper and include the following:

- KEY RESOURCES TABLE
- RESOURCE AVAILABILITY
  - Lead contact
  - Materials availability
  - Data and code availability
- EXPERIMENTAL MODEL AND SUBJECT DETAILS
  - Cells
- METHOD DETAILS
  - Plasmid construction
  - Cytoplasmic and nuclear protein extraction
  - Immunoprecipitation
  - PLA
  - Immunofluorescence
  - Laser micro-irradiation
  - Generation of 3T3 cell lines
  - Colony formation assay
  - Neutral comet assay
  - MNase digestion assay
  - NHEJ and HR reporter assay
  - Cell cycle analysis by BrdU incorporation
- QUANTIFICATION AND STATISTICAL ANALYSIS
  - Statistical analysis

SUPPLEMENTAL INFORMATION

Supplemental information can be found online at https://doi.org/10.1016/j.isci.2021.103676.

AUTHOR CONTRIBUTIONS

DECLARATION OF INTERESTS

The authors declare no competing interests.

REFERENCES

Ahnesorg, P., Smith, P., and Jackson, S.P. (2006). XLF interacts with the XRCC4-DNA ligase IV complex to promote DNA nonhomologous end-joining. Cell *124*, 301–313.

Andres, S.N., Vergnes, A., Ristic, D., Wyman, C., Modesti, M., and Junop, M. (2012). A human XRCC4-XLF complex bridges DNA. Nucleic Acids Res. *40*, 1868–1878.

Attikum, H.v., and Gasser, S.M. (2005). ATP-dependent chromatin remodeling and DNA double-strand break repair. Cell Cycle *4*, 1011–1014.

Bennardo, N., Cheng, A., Huang, N., and Stark, J.M. (2008). Alternative-NHEJ Is a mechanistically distinct pathway of mammalian chromosome break repair. PLoS Genet. *4*, e1000110.

Beucher, A., Birraux, J., Tchouandong, L., Barton, O., Shibata, A., Conrad, S., Goodarzi, A.A., Krempler, A., Jeggo, P.A., and Löbrich, M. (2009). ATM and Artemis promote homologous recombination of radiation-induced DNA double-strand breaks in G2. EMBO J. *28*, 3413–3427.

Calsou, P., Frit, P., Humbert, O., Muller, C., Chen, D.J., and Salles, B. (1999). The DNA-dependent protein kinase catalytic activity regulates DNA end processing by means of Ku entry into DNA. J. Biol. Chem. *274*, 7848–7856.

Caridi, C.P., D'Agostino, C., Ryu, T., Zapotoczny, G., Delabaere, L., Li, X., Khodaverdian, V.Y., Amaral, N., Lin, E., Rau, A.R., et al. (2018). Nuclear F-actin and myosins drive relocalization of heterochromatic breaks. Nature *559*, 54–60.

Ceccaldi, R., Rondinelli, B., and D'Andrea, A.D. (2016). Repair pathway choices and consequences at the double-strand break. Trends Cell Biol. *26*, 52–64.

Chambers, A.L., and Downs, J.A. (2012). Chapter 9-The RSC and INO80 chromatin-remodeling complexes in DNA double-strand break repair. In Progress in Molecular Biology and Translational Science, P.W. Doetsch, ed. (Academic Press), pp. 229–261.

Chen, B.P., Chan, D.W., Kobayashi, J., Burma, S., Asaithamby, A., Morotomi-Yano, K., Botvinick, E., Qin, J., and Chen, D.J. (2005). Cell cycle dependence of DNA-dependent protein kinase phosphorylation in response to DNA double strand breaks. J. Biol. Chem. *280*, 14709–14715.

Critchlow, S.E., Bowater, R.P., and Jackson, S.P. (1997). Mammalian DNA double-strand break repair protein XRCC4 interacts with DNA ligase IV. Curr. Biol. *7*, 588–598.

Davis, A.J., So, S., and Chen, D.J. (2010). Dynamics of the PI3K-like protein kinase members ATM and DNA-PKcs at DNA double strand breaks. Cell Cycle *9*, 2529–2536.

Deng, Z.-H., Gomez, T.S., Osborne, D.G., Phillips-Krawczak, C.A., Zhang, J.-S., and Billadeau, D.D. (2015). Nuclear FAM21 participates in NF-κB-dependent gene regulation in pancreatic cancer cells. J. Cell Sci. *128*, 373–384.

Derivery, E., Sousa, C., Gautier, J.J., Lombard, B., Loew, D., and Gautreau, A. (2009). The Arp2/3 Activator WASH controls the fission of endosomes through a large multiprotein complex. Dev. Cell *17*, 712–723.

Douglas, P., Gupta, S., Morrice, N., Meek, K., and Lees-Miller, S.P. (2005). DNA-PK-dependent phosphorylation of Ku70/80 is not required for non-homologous end joining. DNA Repair *4*, 1006–1018.

Downs, J.A., and Jackson, S.P. (2004). A means to a DNA end: the many roles of Ku. Nat. Rev. Mol. Cell Biol. *5*, 367–378.

Duleh, S.N., and Welch, M.D. (2010). WASH and the Arp2/3 complex regulate endosome shape and trafficking. Cytoskeleton (Hoboken) *67*, 193–206.

Duleh, S.N., and Welch, M.D. (2012). Regulation of integrin trafficking, cell adhesion, and cell migration by WASH and the Arp2/3 complex. Cytoskeleton (Hoboken) *69*, 1047–1058.

Fell, V.L., and Schild-Poulter, C. (2015). The Ku heterodimer: function in DNA repair and beyond. Mutat. Res. Rev. Mutat. Res. *763*, 15–29.

Fritsch, O., Benvenuto, G., Bowler, C., Molinier, J., and Hohn, B. (2004). The INO80 protein controls homologous recombination in arabidopsis thaliana. Mol. Cell *16*, 479–485.

Galarneau, L., Nourani, A., Boudreault, A.A., Zhang, Y., Héliot, L., Allard, S., Savard, J., Lane, W.S., Stillman, D.J., and Côté, J. (2000). Multiple links between the NuA4 histone acetyltransferase complex and epigenetic control of transcription. Mol. Cell *5*, 927–937.

Gerhold, C.B., and Gasser, S.M. (2014). INO80 and SWR complexes: relating structure to function in chromatin remodeling. Trends Cell Biol *24*, 619–631.

Gomez, T.S., and Billadeau, D.D. (2009). A FAM21-containing WASH complex regulates retromer-dependent sorting. Dev. Cell *17*, 699–711.

Gomez, T.S., Gorman, J.A., Artal-Martinez de Narvajas, A., Koenig, A.O., and Billadeau, D.D. (2012). Trafficking defects in WASH-knockout fibroblasts originate from collapsed endosomal and lysosomal networks. Mol. Biol. Cell *23*, 3215–3228.

Hammel, M., Rey, M., Yu, Y., Mani, R.S., Classen, S., Liu, M., Pique, M.E., Fang, S., Mahaney, B.L., Weinfeld, M., et al. (2011). XRCC4 protein interactions with XRCC4-like factor (XLF) create an extended grooved scaffold for DNA ligation and double strand break repair. J. Biol. Chem. *286*, 32638–32650.

Hao, Y.H., Doyle, J.M., Ramanathan, S., Gomez, T.S., Jia, D., Xu, M., Chen, Z.J., Billadeau, D.D., Rosen, M.K., and Potts, P.R. (2013). Regulation of WASH-dependent actin polymerization and protein trafficking by ubiquitination. Cell *152*, 1051–1064.

Hong, X., Li, Z.-X., Hou, J., Zhang, H.-Y., Zhang, C.-Y., Zhang, J., Sun, H., Pang, L.-H., Wang, T., and Deng, Z.-H. (2021). Effects of ER-resident and secreted AGR2 on cell proliferation, migration, invasion, and survival in PANC-1 pancreatic cancer cells. BMC Cancer *21*, 33.

Jia, D., Gomez, T.S., Metlagel, Z., Umetani, J., Otwinowski, Z., Rosen, M.K., and Billadeau, D.D.

(2010). WASH and WAVE actin regulators of the Wiskott–Aldrich syndrome protein (WASP) family are controlled by analogous structurally related complexes. Proc. Natl. Acad. Sci. U S A 107, 10442–10447.

Kapoor, P., Chen, M., Winkler, D.D., Luger, K., and Shen, X. (2013). Evidence for monomeric actin function in INO80 chromatin remodeling. Nat. Struct. Mol. Biol. 20, 426–432.

Kapoor, P., and Shen, X. (2014). Mechanisms of nuclear actin in chromatin-remodeling complexes. Trends Cell Biol. 24, 238–246.

Kienker, L.J., Shin, E.K., and Meek, K. (2000). Both V(D)J recombination and radioresistance require DNA-PK kinase activity, though minimal levels suffice for V(D)J recombination. Nucleic Acids Res. 28, 2752–2761.

Kurimasa, A., Kumano, S., Boubnov, N.V., Story, M.D., Tung, C.S., Peterson, S.R., and Chen, D.J. (1999). Requirement for the kinase activity of human DNA-dependent protein kinase catalytic subunit in DNA strand break rejoining. Mol. Cell Biol. 19, 3877–3884.

Linardopoulou, E.V., Parghi, S.S., Friedman, C., Osborn, G.E., Parkhurst, S.M., and Trask, B.J. (2007). Human subtelomeric WASH genes encode a new subclass of the WASP family. PLoS Genet. 3, e237.

Liu, R., Abreu-Blanco, M.T., Barry, K.C., Linardopoulou, E.V., Osborn, G.E., and Parkhurst, S.M. (2009). Wash functions downstream of Rho and links linear and branched actin nucleation factors. Development 136, 2849–2860.

Lu, H., Pannicke, U., Schwarz, K., and Lieber, M.R. (2007). Length-dependent binding of human XLF to DNA and stimulation of XRCC4.DNA ligase IV activity. J. Biol. Chem. 282, 11155–11162.

Lu, H., Saha, J., Beckmann, P.J., Hendrickson, E.A., and Davis, A.J. (2019). DNA-PKcs promotes chromatin decondensation to facilitate initiation of the DNA damage response. Nucleic Acids Res. 47, 9467–9479.

Mao, Z., Bozzella, M., Seluanov, A., and Gorbunova, V. (2008). Comparison of nonhomologous end joining and homologous recombination in human cells. DNA Repair 7, 1765–1771.

McNally, K.E., Faulkner, R., Steinberg, F., Gallon, M., Ghai, R., Pim, D., Langton, P., Pearson, N., Danson, C.M., Nägele, H., et al. (2017). Retriever is a multiprotein complex for retromer-independent endosomal cargo recycling. Nat. Cell Biol. 19, 1214–1225.

Mizuguchi, G., Shen, X., Landry, J., Wu, W.H., Sen, S., and Wu, C. (2004). ATP-driven exchange of histone H2AZ variant catalyzed by SWR1 chromatin remodeling complex. Science 303, 343–348.

Morrison, A.J., Highland, J., Krogan, N.J., Arbel-Eden, A., Greenblatt, J.F., Haber, J.E., and Shen, X. (2004). INO80 and γ-H2AX interaction links ATP-dependent chromatin remodeling to DNA damage repair. Cell 119, 767–775.

Nakamura, A.J., Rao, V.A., Pommier, Y., and Bonner, W.M. (2010). The complexity of phosphorylated H2AX foci formation and DNA repair assembly at DNA double-strand breaks. Cell Cycle 9, 389–397.

Pierce, A.J., Johnson, R.D., Thompson, L.H., and Jasin, M. (1999). XRCC3 promotes homology-directed repair of DNA damage in mammalian cells. Genes Dev. 13, 2633–2638.

Price, B.D., and D'Andrea, A.D. (2013). Chromatin remodeling at DNA double-strand breaks. Cell 152, 1344–1354.

Ran, F.A., Hsu, P.D., Wright, J., Agarwala, V., Scott, D.A., and Zhang, F. (2013). Genome engineering using the CRISPR-Cas9 system. Nat. Protoc. 8, 2281–2308.

Reid, D.A., Keegan, S., Leo-Macias, A., Watanabe, G., Strande, N.T., Chang, H.H., Oksuz, B.A., Fenyo, D., Lieber, M.R., Ramsden, D.A., et al. (2015). Organization and dynamics of the nonhomologous end-joining machinery during DNA double-strand break repair. Proc. Natl. Acad. Sci. U S A. 112, E2575–E2584.

Richardson, C., Moynahan, M.E., and Jasin, M. (1998). Double-strand break repair by interchromosomal recombination: suppression of chromosomal translocations. Genes Dev. 12, 3831–3842.

Ropars, V., Drevet, P., Legrand, P., Baconnais, S., Amram, J., Faure, G., Marquez, J.A., Pietrement, O., Guerois, R., Callebaut, I., et al. (2011). Structural characterization of filaments formed by human Xrcc4-Cernunnos/XLF complex involved in nonhomologous DNA end-joining. Proc. Natl. Acad. Sci. U S A 108, 12663–12668.

Sarkar, K., Han, S.-S., Wen, K.-K., Ochs, H.D., Dupré, L., Seidman, M.M., and Vyas, Y.M. (2018). R-loops cause genomic instability in T helper lymphocytes from patients with Wiskott-Aldrich syndrome. J. Allergy Clin. Immunol. 142, 219–234.

Schrank, B.R., Aparicio, T., Li, Y., Chang, W., Chait, B.T., Gundersen, G.G., Gottesman, M.E., and Gautier, J. (2018). Nuclear ARP2/3 drives DNA break clustering for homology-directed repair. Nature 559, 61–66.

Shen, X., Mizuguchi, G., Hamiche, A., and Wu, C. (2000). A chromatin remodelling complex involved in transcription and DNA processing. Nature 406, 541–544.

Tsai, C.J., Kim, S.A., and Chu, G. (2007). Cernunnos/XLF promotes the ligation of mismatched and noncohesive DNA ends. Proc. Natl. Acad. Sci. U S A 104, 7851–7856.

Verboon, J.M., Rincon-Arano, H., Werwie, T.R., Delrow, J.J., Scalzo, D., Nandakumar, V., Groudine, M., and Parkhurst, S.M. (2015). Wash interacts with lamin and affects global nuclear organization. Curr. Biol. 25, 804–810.

Wang, Y.G., Nnakwe, C., Lane, W.S., Modesti, M., and Frank, K.M. (2004). Phosphorylation and regulation of DNA ligase IV stability by DNA-dependent protein kinase. J. Biol. Chem. 279, 37282–37290.

Xia, P., Liu, J., Wang, S., Ye, B., Du, Y., Xiong, Z., Han, Z.G., Tong, L., and Fan, Z. (2017). WASH maintains NKp46(+) ILC3 cells by promoting AHR expression. Nat. Commun. 8, 15685.

Xia, P., Wang, S., Huang, G., Zhu, P., Li, M., Ye, B., Du, Y., and Fan, Z. (2014). WASH is required for the differentiation commitment of hematopoietic stem cells in a c-Myc–dependent manner. J. Exp. Med. 211, 2119–2134.

Yang, G., Liu, C., Chen, S.-H., Kassab, M.A., Hoff, J.D., Walter, N.G., and Yu, X. (2018). Super-resolution imaging identifies PARP1 and the Ku complex acting as DNA double-strand break sensors. Nucleic Acids Res. 46, 3446–3457.

Yoo, S., and Dynan, W.S. (1999). Geometry of a complex formed by double strand break repair proteins at a single DNA end: recruitment of DNA-PKcs induces inward translocation of Ku protein. Nucleic Acids Res. 27, 4679–4686.

Yu, Y., Mahaney, B.L., Yano, K., Ye, R., Fang, S., Douglas, P., Chen, D.J., and Lees-Miller, S.P. (2008). DNA-PK and ATM phosphorylation sites in XLF/Cernunnos are not required for repair of DNA double strand breaks. DNA Repair 7, 1680–1692.

Yu, Y., Wang, W., Ding, Q., Ye, R., Chen, D., Merkle, D., Schriemer, D., Meek, K., and Lees-Miller, S.P. (2003). DNA-PK phosphorylation sites in XRCC4 are not required for survival after radiation or for V(D)J recombination. DNA Repair 2, 1239–1252.

Zhao, K., Wang, W., Rando, O.J., Xue, Y., Swiderek, K., Kuo, A., and Crabtree, G.R. (1998). Rapid and phosphoinositol-dependent binding of the SWI/SNF-like BAF complex to chromatin after T lymphocyte receptor signaling. Cell 95, 625–636.

Ziv, Y., Bielopolski, D., Galanty, Y., Lukas, C., Taya, Y., Schultz, D.C., Lukas, J., Bekker-Jensen, S., Bartek, J., and Shiloh, Y. (2006). Chromatin relaxation in response to DNA double-strand breaks is modulated by a novel ATM- and KAP-1 dependent pathway. Nat. Cell Biol. 8, 870–876.

STAR★METHODS

KEY RESOURCES TABLE

REAGENT or RESOURCE	SOURCE	IDENTIFIER
Antibodies		
Rabbit polyclonal anti-WASH	This paper	N/A
Rabbit antiserum against WASH	This paper	N/A
Mouse Monoclonal anti-phospho-Histone H2A.X (Ser139)	Merck Millipore	Cat#05-636; RRID:AB_309864
Rabbit Monoclonal anti- Histone H2A.X	Cell Signaling Technology	Cat#7631; RRID:AB_10860771
Rabbit polyclonal anti-HA tag	Abcam	Cat#ab9110; RRID:AB_307019
Mouse Monoclonal anti-DNA-PKcs	Cell Signaling Technology	Cat#12311; RRID:AB_2797881
Rabbit polyclonal anti-phospho-DNA-PKcs (S2056)	Abcam	Cat#ab18192; RRID:AB_869495
Rabbit polyclonal anti-phospho-KAP1 (Ser824)	Bethyl Laboratories	Cat#A300-767A; RRID:AB_669740
Rabbit polyclonal anti-KAP1	Proteintech Group	Cat#15202-1-AP; RRID:AB_2209890
Rabbit polyclonal anti-Ku70	Proteintech Group	Cat#10723-1-AP; RRID:AB_2218756
Mouse Monoclonal anti-Ku70	Proteintech Group	Cat#66607-1-Ig; RRID:AB_2881967
Rabbit polyclonal anti-Ku80	Proteintech Group	Cat#16389-1-AP; RRID:AB_2257509
Mouse Monoclonal anti-Ku80	Proteintech Group	Cat#66546-1-Ig; RRID:AB_2881908
Mouse Monoclonal anti-GAPDH	Proteintech Group	Cat#60004-1-Ig; RRID:AB_2107436
Rabbit polyclonal anti-NWASP	Proteintech Group	Cat#14306-1-AP; RRID:AB_10638478
Mouse Monoclonal anti-rabbit IgG-HRP	Santa Cruz Biotechnology	Cat#sc-2357; RRID:AB_628497
m-IgGκ BP-HRP	Santa Cruz Biotechnology	Cat#sc-516102; RRID:AB_2687626
Rabbit oligoclonal anti-Histone H3	Theromo Fisher	Cat#711055; RRID:AB_2532782
Rabbit polyclonal anti-WAVE2	Abbkine	Cat#ABP53432
Mouse Monoclonal anti-BrdU	eBioscience	Cat#11-5071-42; RRID:AB_11042627
Rabbit polyclonal anti-mWASH	Gomez et al., 2012	N/A
Chemicals, peptides, and recombinant proteins		
Etoposide	Sigma	Cat#E1383
5-Bromo-2′-deoxyuridine (BrdU)	Sigma	Cat#B5002
Micrococcal Nuclease	New England Biolabs	Cat#M0247S
CK666	MedChemExpress	Cat#HY-16926
Critical commercial assays		
Duolink® In Situ Detection Reagents Red	Sigma	Cat#DUO92008
Duolink anti-mouse PLA probe MINUS	Sigma	Cat#DUO92004
Duolink anti-rabbit PLA probe PLUS	Sigma	Cat#DUO92002
CometAssay® Kit	R&D systems	Cat#4250-050-K
Protein A agarose beads	Sigma	Cat#P5906
Protein G agarose beads	Sigma	Cat#P7700
EZview™ Red anti-HA affinity beads	Sigma	Cat#E6779
Deposited data		
Raw data for IP-MS proteomics	This paper	ProteomeXchange: PXD026512

Continued

REAGENT or RESOURCE	SOURCE	IDENTIFIER
Experimental models: Cell lines		
HEK-293T cells	National Infrastructure of Cell Line Resource	1101HUM-PUMC000091
HeLa cells	National Infrastructure of Cell Line Resource	1101HUM-PUMC000011
3T3 cells	National Infrastructure of Cell Line Resource	1101MOU-PUMC000018
3T3 WASH^KO cells	This paper	N/A
3T3 WASH^WT + vector cells	This paper	N/A
3T3 WASH^KO + vector cells	This paper	N/A
3T3 WASH^KO + WASHr cells	This paper	N/A
3T3 WASH^KO + WASH.ΔVCAr cells	This paper	N/A
HeLa shWASHa cells	Deng et al., 2015	N/A
HeLa shWASHb cells	Deng et al., 2015	N/A
HeLa shControl cells	Deng et al., 2015	N/A
Oligonucleotides		
See Table S2		
Recombinant DNA		
Plasmid: pCMS3.H1p.shWASH/HA-YFP-WASH	Gomez and Billadeau, 2009	N/A
Plasmid: pCMS3.H1p.shWASH/HA-YFP-NLS.WASH	This paper	N/A
Plasmid: pCMS3.H1p.shWASH/HA-YFP-WASH.ΔVCA	Gomez and Billadeau, 2009	N/A
Plasmid: pCMS3.H1p.shWASH/HA-YFP-NLS.WASH.ΔVCA	This paper	N/A
Plasmid: PCI2-F-YFP-NLS	This paper	N/A
Plasmid: PCI2-HA-mCherry-Ku70	This paper	N/A
Plasmid: PCI2-F-YFP-XLF	This paper	N/A
Plasmid: PCI2-F-YFP-DNA-Lig4	This paper	N/A
Plasmid: pSpCas9(BB)-2A-Puro (PX459) V2.0	Ran et al., 2013	Addgene_62988
Plasmid: sgRNA/Cas9 expression construct targeting mouse WASH	This paper	N/A
Plasmid: pCBASceI	Richardson et al., 1998	Addgene_26477
Plasmid: EJ5-GFP	Bennardo et al., 2008	Addgene_44026
Plasmid: DR-GFP	Pierce et al., 1999	Addgene_26475
Plasmid: PCI2-HA-mCherry	McNally et al., 2017	N/A
Plasmid: pLenti6.3	Hong et al., 2021	N/A
Plasmid: pLenti6.3-mWASH-WT	This paper	N/A
Plasmid: pLenti6.3-mWASH-ΔVCA	This paper	N/A
Software and algorithms		
ImageJ	National Institutes of Health	https://imagej.nih.gov/ij/download.html
FlowJo V.10.1	Treestar	N/A
ZEN	Zeiss	N/A
CASP 1.2.3 beta 1	CASP Lab	N/A

RESOURCE AVAILABILITY

Lead contact

Further information and requests for resources and reagents should be directed to and will be fulfilled by the lead contact, Zhi-Hui Deng (deng.zhihui@qmu.edu.cn).

Materials availability

Antiserum, antibody, plasmids and cell lines generated in this study are available from the lead contact upon request without restriction.

Data and code availability

Raw data for IP-MS proteomics experiment can be found on ProteomeXchange under the identifier PXD026512. Any additional information required to reanalyze the data reported in this paper is available from the lead contact upon request.

EXPERIMENTAL MODEL AND SUBJECT DETAILS

Cells

HEK-293T, HeLa and 3T3 cells were purchased from National Infrastructure of Cell Line Resource. Lentivirus-mediated short hairpin RNA (shRNA) for stable WASH knockdown in HeLa cells has been described (Deng et al., 2015). All cells were cultured in DMEM medium supplemented with 10% fetal bovine serum.

METHOD DETAILS

Plasmid construction

To obtain the plasmid YFP-NLS.WASH or YFP-NLS.WASH.ΔVCA, NLS.WASH or NLS.WASH.ΔVCA that has a SV40 large T antigen NLS sequence (CCTAAGAAGAAGCGTAAGGTC) adjacent to the WASH coding sequence was amplified and cloned into the pCMS3.H1p.shWASH/HA-YFP rescue vector as described before (Gomez and Billadeau, 2009). The YFP-NLS plasmid was obtained by annealing two single-stranded DNAs (NLS.f and NLS.r) and inserting into the plasmid PCI2-F-YFP. To obtain the vector mCherry-Ku70, the full-length Ku70 coding sequence was amplified by PCR using HeLa cDNA as template and cloned into PCI2-HA-mCherry vector. The XLF or DNA ligase 4 expressing plasmid was generated by amplifying the XLF or DNA ligase 4 coding sequence using HeLa cDNA as template and cloning into PCI2-F-YFP vector. The sgRNA/Cas9 expression construct targeting mouse WASH was obtained by annealing two single-stranded DNAs (mWASH.sgRNA.f and mWASH.sgRNA.r) and inserting into the plasmid pSpCas9(BB)-2A-Puro (PX459) V2.0. The lentiviral expression vector pLenti6.3-mWASH-WT or pLenti6.3-mWASH-ΔVCA was generated by amplifying the coding sequence of mouse wild type WASH or its deletion mutant lacking VCA domain (Δ367–475 AA) using 3T3 cDNA as template and cloning into pLenti6.3 vector. All sequences of single-stranded DNAs are listed in the Table S2.

Cytoplasmic and nuclear protein extraction

Cells were harvested and washed with Buffer A (10 mM Hepes, 1.5 mM MgCl$_2$, 10 mM KCl and 0.5 mM DTT). Then the cells were resuspended in Buffer B (10 mM Hepes, 1.5 mM MgCl$_2$, 150 mM KCl, 0.1% NP-40, 0.5 mM DTT, 0.5 mM PMSF, 2 mM Na$_3$VO$_4$ and proteinase inhibitors) and allowed to stand on ice for 10 min. The samples were centrifuged at 6500 rpm for 3 min at 4°C and the supernatants were collected as cytoplasmic extraction. The nuclear pellets were washed with Buffer A containing protease inhibitors twice and collected by centrifugation. The nuclear pellets were resuspended in Buffer C (10 mM HEPES, 25% glycerol, 420 mM NaCl, 1.5 mM MgCl$_2$, 0.2 mM EDTA, 0.5 mM DTT, 0.5 mM PMSF, 2 mM Na$_3$VO$_4$ and proteinase inhibitors) and incubated on ice for 30 min. Samples were centrifuged at 12000 rpm for 10 min at 4°C and the supernatants were collected as nuclear extraction. The nuclear extract for immunoprecipitation was diluted with two volumes ice-cold Buffer A containing protease inhibitors and subjected to the subsequent immunoprecipitation.

Immunoprecipitation

Cells were harvested and then lysed with lysis buffer (20 mM Hepes pH7.2, 50 mM Potassium Acetate, 200 mM D-sorbitol, 1 mM EDTA, 0.1% Triton X-100, 0.5 mM PMSF, 2 mM Na$_3$VO$_4$ and proteinase inhibitors) on ice for 30 min. After centrifugation, the clarified lysates were incubated with the normal rabbit serum or antiserum against WASH in the presence or absence of EtBr (0.2 mg/mL) overnight, followed by incubation with protein A and protein G agarose beads at 4°C for 1 hr. The beads were washed with lysis buffer five times and analyzed by immunoblot. For HA- immunoprecipitation, whole cell lysates, cytoplasmic or nuclear extracts were incubated with EZview™ Red anti-HA affinity beads overnight at 4°C. Precipitates were then washed and immunoblotted with the indicated antibodies or subjected to mass spectrometry.

PLA

Cells grown on cover slips were fixed, permeabilized and then subjected to *in situ* PLA using Duolink Detection Reagents Red (DUO92008, Sigma) according to the manufacturer's instructions. Duolink anti-mouse PLA probe MINUS (DUO92004, Sigma) and Duolink anti-rabbit PLA probe PLUS (DUO92002, Sigma) were used. Hoechst 33342 staining was performed to visualize nuclear DNA.

Immunofluorescence

Cells cultured on glass bottom dishes were treated with 50 μM etoposide for 0, 15, 30, 60 or 120 min, and in some cases were allowed to recover for 0 or 24 hr under normal growth conditions. Cells were fixed, permeabilized, blocked with IF blocking buffer (5% goat serum, 1% glycerol, 0.1% BSA, 0.1% fish skin gel and 0.04% sodium azide in PBS buffer) and incubated with primary antibody overnight. Subsequently, samples were washed and incubated with secondary antibody at room temperature for 1 hr in the dark. After washing with PBS, Hoechst 33342 staining was performed to visualize nuclear DNA. Images were acquired using Zeiss LSM-710 laser scanning confocal microscope integrated with Zen software utilizing 63× oil objective lens and analyzed using ImageJ software.

Laser micro-irradiation

For real-time recruitment of fluorescent proteins, YFP-tagged constructs and/or mCherry-Ku70 were transfected into HEK-293T cells which were plated on 24-well glass bottom plates. Transfected cells were incubated in medium containing 20 μM BrdU for at least 24 hr prior to micro-irradiation experiment and the medium was replaced by cell medium without phenol-red before micro-irradiation. Localized DNA-damage was generated by irradiating a stripe of 10-pixel width with a 405 nm laser using FRAP module of the ZEN software (405 nm laser set to 70%). For DNA damage induction followed by immunofluorescence staining, cells were incubated in medium containing 10 μg/mL Hoechst 33,342 for 10 min instead of the BrdU treatment prior to micro-irradiation experiment. DNA-damage was generated by micro-irradiation with a 405 nm laser using FRAP module of the ZEN software (405 nm laser set to 92%). Three or five minutes after micro-irradiation, cells were fixed and subjected to immunofluorescence. The fluorescence intensity of laser-generated damaged tracks was measured with ImageJ software and normalized to that of a control area. All results represent images of more than twenty-five cells from three independent experiments.

Generation of 3T3 cell lines

WASH^KO 3T3 cell line was generated using CRISPR/Cas9 gene editing. The sgRNA/Cas9 expression construct was transiently transfected into 3T3 cells. Twenty-four hours after transfection, cells were treated with puromycin for 48 hr prior to being plated to acquire individual clones. WASH^KO cells were validated by immunoblot. To produce lentiviral particles, HEK-293T cells were co-transfected with pLenti6.3-mWASH-WT, pLenti6.3-mWASH-ΔVCA or pLenti6.3 empty vector with psPAX2 and pMD2.G. Forty-eight hours after transfection, the lentiviral particles were obtained by harvesting the media from the cells. WASH^WT and WASH^KO 3T3 cells were transduced with the indicated lentiviral particles, and were selected using 2 μg/mL blasticidin for 10 days.

Colony formation assay

Cells treated with the indicated concentration of etoposide for 6 hr were plated on 6-well plates at a cell density of 500 cells per well. After 7 days, cells were stained with 0.1% crystal violet. Colonies were scored and the cell survival fractions were normalized to untreated controls of the corresponding cells.

Neutral comet assay

Cells were treated with 50 μM etoposide for 1 hr and allowed to recover for 30 min under normal growth conditions. Cells were then subjected to neutral comet assay using the CometAssay® Kit (4250-050-K, R&D systems) according to the manufacturer's instructions. CASP Comet Assay Software was used to automatically analyze the comets and calculate the Tail moments.

MNase digestion assay

Cells grown in 10 cm dishes were treated with 50 μM etoposide for 1 hr. After harvesting, cells were washed with cold PBS and resuspended in cold hypotonic Hank's balanced salt solution (HBSS) buffer (340 mM sucrose, 15 mM Tris, pH 7.5, 15 mM NaCl, 60 mM KCl, 10 mM DTT, 0.15 mM spermine, 0.5 mM spermidine and 0.5% Triton X-100). After incubation on ice for 10 min, the nuclei were pelleted via centrifugation at

11000 rpm for 5 minutes, washed with HBSS buffer, resuspended in 1:1 HBSS/glycerol and stored at - 20°C overnight. Then the nuclei were centrifuged and resuspended in 70 μL MNase digestion buffer (250 mM sucrose, 15 mM Tris, pH 7.5, 15 mM NaCl, 60 mM KCl, 0.5 mM DTT and 1 mM $CaCl_2$). The nuclei suspension of each sample was incubated at 37°C for 5 min after adding 2 μL 20 gel unit/μL MNase and the digestion reaction was stopped by adding 2 μL of 0.5 M EDTA. After incubation with 2 μg/μL RNase A at room temperature for 5 min, 8 μL of 5% SDS with 1 mg/mL Proteinase K was added to each sample and that was then incubated at 37°C for 30 min. The DNA was extracted with phenol/chloroform/isoamyl-alcohol and precipitated with ethanol and sodium acetate. 3 μg of each sample was separated on a 1.2% agarose gel electrophoresed in Tris-acetate EDTA buffer, stained with EtBr, and visualized via the GE Amersham Imager 680. The DNA band intensity of each gel lane was quantified with ImageJ software and normalized to total intensity of the whole lane.

NHEJ and HR reporter assay

HEK-293T cells grown on 6-well plates were transiently transfected with 1 μg pCBASceI, 1 μg PCI2-HA-mCherry and either 1 μg EJ5-GFP or DR-GFP 24 hr after the transfection of the indicated siRNAs. Seventy-two hours after transfection, flow cytometry analysis was performed to detect GFP and mCherry-positive cells using a FACS Calibur flow cytometer (BD Biosciences) and FlowJo software. mCherry-positive cells served as a control for transfection efficiency. NHEJ efficiency was calculated by comparing the number of GFP-positive cells with the number of mCherry-positive cells.

Cell cycle analysis by BrdU incorporation

The cell proliferation analysis was performed as previously described (Hong et al., 2021). WASH[WT] and WASH[KO] 3T3 cells at about 80% confluence were treated with 30 μM BrdU for 30 min at 37°C. Then cells were fixed, acid-treated, and detected using FITC-conjugated anti-BrdU antibody. The DNA was stained with 20 μg/mL of propidium iodide (PI). All samples were analyzed using a FACS Calibur flow cytometer (BD Biosciences) and FlowJo software.

QUANTIFICATION AND STATISTICAL ANALYSIS

Statistical analysis

Statistical analysis was performed using the Student's t test (unpaired, two-tailed) for two groups and one-way or two-way analysis of variance (ANOVA) with Dunnett's multiple comparisons test for multiple groups in GraphPad Prism. Details of statistical analysis method and information including n, mean, and statistical significance values are indicated in the corresponding sections of the figure legends or methods. Experiments were replicated three times and bar plots represent mean ± S.E.M. or mean ± S.D. as indicated. $p < 0.05$ was considered significant. $*p < 0.05$, $**p < 0.01$, $***p < 0.001$, $****p < 0.0001$; n.s., not significant.